



Sea-ice ridges are a major component of Arctic sea-ice export through the Fram Strait

Dmitry V. Divine¹, Sebastian Gerland¹, and Mats A. Granskog¹

¹Norwegian Polar Institute, Fram Centre, Tromsø, Norway

Correspondence: Dmitry V. Divine¹ (dmitry.divine@npolar.no)

Abstract.

This study presents seven years (2012-2019) of Arctic sea-ice draft observations from upward-looking sonars combined with coincident observations of ice drift velocity from four moorings located across the Arctic outflow in the Fram Strait at 78.83°N. The data set covers in total about 150 000 km of drifting Arctic sea ice, at a 1 m spatial resolution, providing one of the most extensive spatially referenced sea-ice draft records in the Arctic available today. Level ice makes up about 40-50% of the ice cover, with modal ice thickness varying between 1 m and 2.5 m, and thicker level ice westward towards the east Greenland shelf. Using local level-ice thickness and a variable-threshold ridge detection algorithm, we identify and quantify the sizes of sea-ice ridges, including shallow ridges with keel drafts less than 5 m deep, often overlooked by traditional methods using a fixed threshold. The study highlights ridges as a significant component of the sea-ice cover, with keels covering some 20–30% of the ice bottom and contributing 28–55% of the total sea-ice volume. The typical spatial density varies from 6 to 9 individual ridges per kilometer of sea-ice, with approximately 3000 to 5500 ridges per month at each site. A westward increase in ridge frequency and coverage was associated with the differences in the origin of sea ice arriving at the mooring locations. Further, we show that shallow ridges comprise up to 80% of all ridges and 35–45% of the ridged ice volume, and thus play an important role in the sea-ice volume budget. Thus, shallow ridges deserve greater attention, especially given the ongoing changes in the Arctic sea-ice cover.

1 Introduction

In polar regions, understanding the spatial and temporal variability in the thickness and extent of sea ice is crucial in various disciplines such as oceanography, meteorology, marine biology, and engineering. A large fraction of the sea-ice cover resides in ridges (e.g. Wadhams, 1990; Melling and Riedel, 1996; Hansen et al., 2014), dynamically formed structures that make up the thickest part of the Arctic ice pack, which is arguably the least studied component of Arctic sea ice.

Sea ice, being the interface between the atmosphere and ocean, crucially affects the interactions between the two. In this context, sea-ice ridges play a crucial role in the transfer of momentum from the atmosphere to the ocean due to their contribution to the ice-atmosphere and ice-ocean drag (e.g. Arya, 1973; Lu et al., 2011; Castellani et al., 2014; Brenner et al., 2021). Sea ice is also an integral part of the polar marine ecosystem, and sea-ice ridges, though understudied, are considered possible biological hotspots or refuge for ice-associate organisms when thinner ice melts (Gradinger et al., 2010; Fernández-Méndez





et al., 2018). In the realm of engineering, ridges pose the highest loads on ships, coastal and offshore structures, influencing ice navigation, offshore operations, and the design and construction of marine structures (Polojärvi et al., 2025).

Fram Strait is the main gateway that connects the Arctic Ocean and the North Atlantic Ocean, where almost 90% of the sea-ice export from the Arctic Ocean occurs (e.g. Spreen et al., 2020; Sumata et al., 2022). The ice transported to Fram Strait represents a broad range of thicknesses and types and exhibits an integrated dynamic-thermodynamic history on its way across the Arctic before reaching Fram Strait (Vinje et al., 1998; Hansen et al., 2013; Sumata et al., 2023). This makes the area a suitable location to monitor the state of Arctic ice pack and Upward-Looking Sonars (ULS) in combination with Acoustic Doppler Current Profilers (ADCP) measuring sea-ice draft and sea-ice velocity have become essential components of the Fram Strait Arctic Outflow Observatory. Maintained by the Norwegian Polar Institute, the array of several taut-line moorings has operated since 1990 (Vinje et al., 1998), providing a unique and nearly seamless record of key characteristics of drift ice on its main pathway out of the Arctic Ocean (Hansen et al., 2013; Sumata et al., 2023). Over three decades of operation, they have captured changes in the state of the Arctic sea ice. Overall shrinking of the Arctic sea-ice cover has left a clear imprint on the recorded ice draft (and hence ice thickness) in the Fram Strait. In particular, data from the Arctic Outflow Observatory provided clear evidence of thinning of the Arctic ice cover (Hansen et al., 2013; Sumata et al., 2023), both in terms of the mean and shape of the probability density function (PDF) of sea ice thickness, further linked to a change in the age structure of Arctic sea ice (Sumata et al., 2023).

While there is a wealth of data collected on sea-ice draft from moored observations, only a few so far have been referenced in space. A time-series of ice draft can be converted to a spatial (or distance) series along the ice drift trajectory through a combination with in situ, for example ADCP-based, ice velocity time-series (Melling et al., 1995). Given that the time resolution of both input data series is sufficiently high, that is, $\mathcal{O}(1sec)$ for the draft and $\mathcal{O}(60sec)$ for the velocity, this enables reconstruction of the sea-ice bottom topography at a meter-scale spatial resolution. Such data in turn allow isolation of individual features in ice cover, such as ridges or segments of level ice, hence disentangling the contributions of different ice classes/ice categories into the ice thickness distribution. Furthermore, partitioning the volumetric fractions of different ice categories within the total ice mass budget allows estimation of their individual contributions to sea-ice and hence freshwater fluxes. Knowledge of ridge frequency, keel depth distribution and keel configuration is also crucial for building credible ice—ocean drag parameterizations to be used in climate models (Tsamados et al., 2014; Sterlin et al., 2023; Brenner et al., 2021). This can also be important in a number of practical applications, for example engineering where knowledge of the temporal frequency of ridges and their maximum depth at a given site may suffice (Wadhams, 1983, 2012; Samardžija and Høyland, 2023). In remote sensing, the areal ridge fraction or ridge density is useful for validation of satellite-based retrievals of the properties of the sea-ice cover (e.g. Duncan and Farrell, 2022; Mchedlishvili et al., 2023; Ricker et al., 2023), important for both scientific applications as well as navigation in ice covered waters.

However, most of the few existing studies (with spatially referenced data) are either from peripheral Arctic seas that arguably observe local ice conditions or over shorter periods of time (e.g. Melling and Riedel, 1995; Melling and Riedel, 1996; Brenner et al., 2021; Valenti et al., 2021). For the Fram Strait, attempts to combine ice draft and ice velocity were made earlier, but with sea-ice velocity estimates based on sea-ice drift modeling or from remote sensing, inducing rather large uncertainties (Ekeberg





et al., 2014, 2015). However, since 2012, ULS deployments in the Fram Strait have typically been accompanied by ADCP deployments configured to simultaneously record ice velocity, making it possible to convert sea-ice draft time-series data into accurate spatial series (cf. Melling et al., 1995).

This study uses high-resolution sea-ice draft measurements and coincident ADCP ice velocity measurements obtained from moorings of the Fram Strait Arctic Outflow Observatory over a seven-year period (2012-2019), located in the core of the East Greenland Current. The available spatial series of sea-ice draft are used to categorize level and deformed ice, identify sea-ice ridges, and to examine their seasonal and interannual variability in terms of their number, frequency, and estimate their areal and volumetric contributions to the sea-ice cover in the Arctic outflow area.

2 Data and Methods

2.1 ULS sea-ice draft data series

Sea-ice draft data series from September 2012 to September 2019 were obtained from four ULSs moored in the East Greenland Current in the western Fram Strait. ULSs are deployed at the top of the mooring line at around 50 m below the water surface, independent of the local water depth. The moorings are aligned zonally at approximately 78.83°N and make a transect from the core of the East Greenland Current to the edge of the east Greenland shelf. The zonal positions of the ULS-equipped moorings and the naming conventions used for the moorings are as follows: F11 at 3°W, F12 at 4°W, F13 at 5°W and F14 at 6.5°W (Figure 1). General information on the moorings is further summarized in Table 1.

The moorings are serviced annually during a cruise to the area, typically in August-September, which is also a period of the regional sea-ice minimum. Time intervals between the recovery and re-deployment were typically between one to two weeks, on average, ensuring minimal possible temporal gaps in the series. However, some hiatuses in the data series were also present due to instrument malfunctions or losses of the moorings. Figure 2 shows the timelines/overview of the available data for the four moorings for the considered period.

An ULS measures the return travel time of an acoustic pulse reflected off the underside of the sea ice. This return time can be converted to an acoustic range value by using the speed of sound in seawater, resulting in the ice draft. More details on the principles of operation, including typical data processing procedures and the associated uncertainties for the retrieval of the target parameters can be found elsewhere (e.g. Melling and Riedel, 1995; Fissel et al., 2008). In the study period, ULS data was acquired using IPS5 instruments (Ice Profiling Sonar model 5) from ASL Environmental Sciences. The entire data set was then processed by ASL following the methodology of Melling and Riedel (1995) and Fissel et al. (2008), also described in Hansen et al. (2013). Specific technical information on the instruments is available from the manufacturer (http://www.aslenv.ca).

The sampling rate of the instruments was set to 2 s, corresponding to ca. 1.3×10^6 ice draft observations per month. For an IPS5 installed at a nominal depth of 50 m, the footprint of the sonar beam has a diameter of about 1.8 m. For typical sea-ice drift velocities of up to 1 kn (about 0.5 m s⁻¹) observed in the Fram Strait, such a sampling rate ensures an overlap of beam footprints and therefore a continuous sampling of the ice surface. The actual depth of the instruments might vary though, both due to slightly different settings between different deployments, and during particular season in response to the variable ocean



100

105

110

125



drag. The theoretical error of the sonar derived drafts is, according to manufacturer data sheets, claimed to be within ± 0.05 m. However, various errors may accumulate during processing due to errors inherent in the input of auxiliary data necessary in the processing routines, such as local sea level pressure and instrument tilt. Furthermore, additional uncertainties emerge at the stage of data interpretation in the speed of sound estimates based on detected open water events, beam width/footprint effects, waves penetrating through the ice, and false targets like gas bubbles in the water or even various biological objects. Therefore, the accuracy of each draft measurement is typically about 0.1 m. The uncertainty of each individual measurement is considered not to be subject to bias errors and the summary error statistics of monthly values should be well below 0.1 m.

The ice draft is sampled at regular time intervals but due to the irregular motion of the ice cover the resulting series is unevenly spaced in distance relative to sea-ice surface. To account for this, the ice draft time series were further augmented with sea-ice velocities to generate a spatially uniform series of ice draft. Ice velocity measurements were made with an ADCP (Teledyne RDI Acoustic Doppler Current Profiler), deployed on the moorings some 8 m below the ULSs. The ADCPs recorded ice velocities at 20-minute sample intervals. These were averaged and used in a double-weighted double-quadratic interpolation scheme to a yield series of sea-ice draft with a spatially uniform increment of 1 m.

Figure 2 demonstrates that the temporal coverage of the spatially resolved sea-ice series is lower than for the available ice draft data, which is mainly related with the lack of sea-ice velocity data due to, e.g., instrument failures. The total lengths of the analyzed data records, i.e. distance of sea ice tracked at each mooring location, therefore, varies. The longest and almost seamless series covering about 46 000 km of sea-ice draft and velocity is available from the F11 mooring (see Fig. 2 and Table 1). The re-sampled spatial series were then used in ice ridge and level ice identification procedures and also enabled calculation of various spatial metrics characterizing spatial and size distributions of ridges and their areal and volumetric contributions to sea-ice cover in the area.

2.2 Detection of ridges and level ice

Algorithms to detect/isolate individual ridges from ice draft profiles acquired by submarine sonars or sea-bottom anchored moorings were applied in a number of previous studies (e.g. Williams et al., 1975; Wadhams and Horne, 1980; Wadhams and Davis, 2000; Melling and Riedel, 1996; Wadhams et al., 2011; Ekeberg et al., 2015; Hansen et al., 2023). Ridges were typically identified using the Rayleigh criterion with level ice draft threshold of 2.5 m and a minimum ridge keel draft of 5 m (see e.g. Ekeberg et al., 2015, for a graphical depiction of the procedure), though the constant level ice threshold value varied between studies. The criterion in these studies defines an individual ice ridge when the ice thickness on each side of a local maximum descends at least halfway toward the threshold of level ice draft, which is meant to be sufficiently high to avoid deformed or level ice to be identified as ridges, while a minimal ridge keel draft of 5 m is set to exclude rafted ice.

However, the use of constant thresholds represents a weakness of this approach as it prevents the detection of ridge keels with a draft less than 5 m, which are known to be numerous (e.g. Timco and Burden, 1997). A constant 2.5 m threshold for level ice often used for identification and isolation of ridges in sea-ice draft series was a reasonable approximation in the past when the Arctic sea-ice was generally thicker than today. The ongoing thinning and substitution of older ice by first-year and younger ice would lead to an underestimate in the number of detected ridges. The decrease in mean modal level ice thickness



130



in the Fram Strait to less than 2.5 m became apparent already after the major 2006 summer Arctic sea ice minimum (Hansen et al., 2013, 2014) and has continued to decline since then (Sumata et al., 2022, 2023). Together with increased seasonality in level ice thickness in the area, it suggests that the use of constant thresholds in ridge detection would lead to a seasonally and temporally variable bias in the number of detected ridges.

To account for a variable level ice draft for ice ridge detection, the modified scheme should, therefore, involve a level ice identification procedure. We use the approach of Wadhams and Horne (1980) that defines level ice through a local ice draft gradient that is set to be less than $0.025 \,\mathrm{m}^{-1}$. In addition, we set an upper limit of 2.5 m for local level ice draft which roughly corresponds to the limit of thermodynamic sea-ice growth (e.g. Maykut and Untersteiner, 1971). In order to minimize the effect of individual spikes/jitter in ice draft series on level ice detection, a 3-meter running average was applied to the series prior to the level ice identification procedure. Smoothing was retained only for the data segments associated with level ice, while the ridge detection procedure was applied to the original spatial draft series. The ridge detection algorithm is then applied in the next step with the ice draft threshold defined locally using the linearly interpolated level ice thickness on both sides of the potential ridge keel draft being tested. The approach we apply in this study is similar to the method recently used in Brenner et al. (2021). A main difference is found in level ice draft which in Brenner et al. (2021) is a 17-minute (or "ADCP-burst" based) median of all ice segments identified as level ice, while it is a local variable in our approach. We also set a minimum ridge keel draft of h_{kmin} of 2 m to filter out ice rubble.

Figure S1 illustrates the output of the approach showing a few randomly selected examples of ice ridges of different shapes and dimensions identified using ridge and level ice identification schemes. Note that since the spatial orientation of ridges relative to sea-ice drift direction is not available from this type of data, the actual (true) keel widths of individual ridges can not be inferred from the identified ridge cross-sections.

2.3 Distributions of ridge keel drafts and ridge density

Previous studies on the ridge keel draft probability density demonstrates that it generally follows an exponential distribution (e.g. Wadhams and Davy, 1986). Alternatively, Hansen et al. (2023) applied a heavy-tailed Weibull distribution for the same purpose that due to its two-parameter functional form may provide a better fit. In this study, we rely on the exponential form of the probability density of the ridge keel draft probability density given its simplicity and suitability to represent our data. It is also assumed that the exponential form of the keel draft PDF is also suitable for ridges with a keel shallower than 5 m (referred hereafter as "shallow keels"). Since we set a lower limit of $h_{kmin} = 2$ m on ridge keel draft, for a more accurate formalization, a shifted exponential distribution form is applied:

$$f(x;\lambda) = \lambda e^{-\lambda(x - h_{k min})}, \quad x \ge h_{k min}, \lambda > 0$$
(1)

where λ is the rate parameter, also linked to the mean $(h_{kmin} + 1/\lambda)$ and median $(h_{kmin} + ln2/\lambda)$ of the distribution. The cumulative density function (CDF) for the distribution is expressed as:

$$F(x;\lambda) = 1 - e^{-\lambda(x - h_{kmin})}, \quad x \ge h_{kmin}, \lambda > 0$$
(2)





Fitting a single parameter exponential distribution to the data subsets therefore represents a convenient way of analyzing and highlighting both seasonal and interannual variability in ridge keel drafts. Given the known h_{kmin} , the rate parameter λ of the exponential distribution can be derived using maximum likelihood estimator (MLE) on the subsets of ridge keel drafts over time (or ice distance) intervals of interest (Arnold, 1990).

The number of keels per km of ice, also often referred to as "ridge density" or "ridge frequency", can be approximated by a log-normal form (e.g. Wadhams and Davy, 1986; Tan et al., 2012):

$$f(x;\mu,\sigma) = \frac{1}{x\sigma\sqrt{2\pi}} \exp\left(-\frac{(\ln x - \mu)^2}{2\sigma^2}\right), \quad x > 0$$
(3)

where μ and σ are the mean and the standard deviation of the natural logarithm of the analyzed variable, respectively. The values of μ and σ can be used to calculate the median ridge density (e^{μ}) and its 68% prediction intervals of [$e^{\mu/\sigma}$, $e^{\mu*\sigma}$] from the log-normal probability distribution fitted to the data segment of interest. Note that we specifically report the median rather than the mean values for the fitted distributions, since the median is known to be a more robust estimator of central tendency in skewed distributions (e.g. Tukey, 1977).

3 Results and Discussion

170

185

190

The presented approach to isolate ridges and level ice segments effectively splits the spatial series of ice drafts into three major ice categories: level ice, ice ridges and mixed. The latter is a residual variable and combines all types of sea ice that could not be associated with the other two categories. This can be, for example, shallow ice rubble fields or segments of ice identified as level but with a thickness that exceeds the thermodynamic threshold of 2.5 m and hence possibly being of dynamic origin. Open water was identified already at the stage of initial data processing. However, to account for the uncertainty in the draft series data, the data segments identified as ice with a thickness of less than 0.05 m were treated as open water in the analysis. Note that here and below, the derived values for identified ice ridges and ice categories such as counts or areal fractions are often presented relative to the ice surface only, i.e., with open water segments excluded. These are specifically referred to as "effective" values.

3.1 Variations in fractional coverage of level and deformed ice

Figure 3 shows a time series of the distribution of level ice, ice ridges and mixed for the four moorings from 2012 to 2019. The results are presented as monthly areal fractions, though they are essentially fractions in terms of the total distance ice drifted over a mooring during the period specified. Figure 3 shows that the areal fractions of the ice categories are similar between the moorings, with level ice making up approximately 40-45% of the ice area and the rest associated with deformed ice types. This is in line with observations made in May 1987 from a submarine in the Fram Strait and Greenland Sea, when Wadhams (1992) reported level ice fractions of 35-49%. While late summer submarine observations (1958 and 1970) in the central Arctic Basin (covering about 2000 km each year), upstream of Fram Strait, indicated level ice fractions of about 50-55% (McLaren, 1988, 1989). Williams et al. (1975) analyzed submarine data from March 1971 between 85 and 90°N (560 km of track), north





of Fram Strait, and indicated typical level ice fractions of 30% (range 13 to 49% for 10 km segments). Also north of Fram Strait, from a submarine survey in October 1976, Wadhams (1981) reported about 50% level ice fraction. Wadhams and Horne (1980) reported the fraction of level ice from spring 1976 in the Beaufort Sea from 1400 km of submarine track to be 56%. Kortum et al. (2024) in a more recent study based on MOSAiC airborne data showed 50% level ice fractions, though the analysis focused specifically on FYI. Other studies where level ice fraction was defined as a residual variable (i.e. calculated based on the deformed ice fraction) pointed to a substantial variability in level ice coverage between seasons, regions and ice categories, as well as in response to the methods used, thus direct comparison to other studies is not always straightforward. We note also that due to a relative short temporal coverage of the analyzed data and substantial seasonal and interannual variability, no significant changes in the areal fractions in any of the three ice categories were evident over the study period.

200 3.2 Variability of level ice draft

205

210

220

Figure 4 shows the temporal variability of the probability density of level ice draft in Fram Strait over the study period for the four moorings. For a better visualization the monthly PDFs that aggregates all level ice segments for a particular month are displayed. The PDFs are typically bimodal, with a second maximum associated with the modal ice thickness (Hansen et al., 2013; Sumata et al., 2023). In order to highlight the modal thickness of level ice, a peak detection algorithm was applied to the data to identify the maximum in ice thickness PDF for sea ice thicker than 0.7 m, which corresponds to FYI of medium thickness and thicker and/or older ice types (JCOMM Expert Team on Sea Ice, 2015). The first peak below this threshold typically emerges during the late fall-early winter to early summer (mid-October to early June) linked to thickness evolution of younger ice formed during the freezing season. The seasonal cycle in this thinner ice is more pronounced at F13 and F14, located more to the west inside the ice pack. While the thicker ice is the ice transported from the Arctic basin, the thinner ice is more likely to correspond to younger sea ice that has formed locally or just upstream of the mooring locations.

The modal ice thickness shows substantial interannual variability between 1 m and 2.5 m during the study period, with a tendency for thicker level ice towards the west, i.e. closer to Greenland. There are clear similarities in the patterns of interannual variations between all four series as as well evidence of coherent features in level ice thickness variability at subannual time scales. One can note, for example, that a pronounced increase in modal ice thickness occurred from late spring to early fall of 2019 - a downstream effect of winter 2018-2019 Arctic sea-ice thickness anomalies (Kacimi and Kwok, 2022; Richter-Menge et al., 2019), potentially occurred in response to increased sea-ice residence time in the Arctic basin in the previous two years (Sumata et al., 2023).

Figure 4 also confirms that the fixed 2.5 m level ice draft threshold for ice ridge detection in modern ice conditions would be too conservative. Level ice attained a modal thickness of 2.5 m in only a few occasions during the study period, which would therefore led to under-counting/under-identification of ridges if the scheme with a fixed threshold was applied (see Section 3.3 for details).



225

230

235

240

245

250



3.3 Ice ridge density and monthly ridge number variability

Figure 3 showcase ice ridges as ubiquitous objects comprising a substantial part of sea-ice cover in Fram Strait, with a series-average fractional areal coverage of 20-30%. Figure 5 further shows the daily effective spatial ridge density (also referred as ridge frequency), calculated from the daily number of detected ridges divided by the daily horizontal distance of sea ice that drifted over the mooring. For the observed ice drift speeds in the Fram Strait (e.g. Sumata et al., 2022) this distance should typically be less than 20 km. The effective ridge density can be as high as 30 ridges per km sea ice. Note that the periods of open water, shown in Fig. 5 as monthly values for a better visualization, were excluded from these calculations.

Figure 6 combines the daily effective density of ridges for each mooring into a single probability distribution. The daily ridge density has a right-skewed distribution that is well approximated by a log-normal form (Wadhams and Davy, 1986; Tan et al., 2012). The respective median frequencies for each site were estimated from the fitted distributions together with their prediction intervals and presented in Table 2. The medians are similar to the recent estimates of 6-15 ridges km⁻¹ from Krumpen et al. (2025) from airborne data, for sea ice in the Transpolar Drift (TPD), upstream of Fram Strait, but much higher than the estimates of less than 3.6 (mean) or 1.2 (median, calculated from the provided parameters of the Weibull distribution) ridges km⁻¹ for the Barents Sea ice cover over a nearly identical period 2014-2020 (Hansen et al., 2023). However, the locations in the Barents Sea were typically dominated by younger and thinner ice, which should have experienced a shorter deformation history.

Figure 6 demonstrates a tendency for a higher density of ridges towards the west, with the median ridge frequency of $6 \,\mathrm{km^{-1}}$ at $3^{\circ} \mathrm{W}$ (F11), increasing to about $10 \,\mathrm{km^{-1}}$ at $6.5^{\circ} \mathrm{W}$ (F14). The difference is, however, confined to the 68% prediction intervals of the fitted log-normal distributions.

In agreement with Krumpen et al. (2025), the density of ridges does not show any clear seasonal patterns at any of the four mooring sites (see Fig. S4). Hence, the observed gradient in the ridge density across the East Greenland Current can not be explained only by seasonal sea-ice melt and its possible effect on the ridge detection scheme, which would be more pronounced at F11 compared to F14. The increased ridge frequency towards west is most likely to be attributed to the differences in the prevalent source regions of sea ice for the mooring locations (Sumata et al., 2023). More specifically, the sites located to the west tend to receive a higher fraction of ice originating from the TPD and the Canadian Arctic. This ice is generally characterized by a greater proportion of older ice types, suggesting an extended deformation history and hence increased ridge coverage (Krumpen et al., 2025; Duncan and Farrell, 2022).

Figure 7 shows monthly ridge counts and monthly effective ridge counts (ridge counts scaled/divided by monthly sea ice concentration) together with their multiannual means and respective standard deviations. The figure summarizes variability in the number of ridges that drifted over the moorings over the study period. The period averages for ridge counts are also found in Table 2. The numbers of monthly effective ridge counts gradually increase from about 4000 at F11 to 5500 at F14, yet the interannual variability is large, with highest counts attaining some 12 000 ridges a month.

The monthly average of 5500 ridges for F14 is similar to the estimates of Ekeberg et al. (2014) for the period 2006-2008 at F14, and does not follow the rapid decline in monthly ridge counts down to about 2000-3000 observed later in 2009-2011 and



265

270

275

280

285



associated with a shift in the structure/composition of Arctic sea ice after the 2007 summer minimum Ekeberg et al. (2014). However, Ekeberg et al. (2014) used a threshold of 5 m for the keel draft in the ridge detection procedure, along with a constant level ice thickness threshold of 2.5 m, indicating that this scheme likely undercounted ridges with a keel shallower than 5 m. Analysis of the derived keel-depth distributions and its temporal variability shows that shallow ridges constitute on average 60-70% of all detected ridges (Figure 7, see also Fig. S2 where the ridge counts with variable and fixed thresholds are compared). This makes our estimates of the series-average ridge count for F14 for ridges with keels >5 m deep of about 2000 ridges a month consistent with the results of Ekeberg et al. (2014) for the 2006-2011 period.

We note that a linear regression analysis applied to effective monthly ridge counts suggests that there was a decrease in the number of ridges at the four sites (Figure 7). This decline is statistically significant only at F12 and, to some extent, can be associated with the effect of a pronounced Arctic sea-ice outflow minimum around 2018 (Sumata et al., 2022). The decreasing number of ridges over the study period, when placed in the context of a higher ridge count observed before, therefore extends the tendency found in Ekeberg et al. (2014) for the preceding period of 2006-2011 and generally in line with findings of Krumpen et al. (2025) for ridge density in the TPD for a longer period of 1993-2023 from airborne data. However, the actual trend magnitudes are difficult to establish given the shortness and hiatuses in the data series, as well as large interannual variability.

3.4 Keel draft variability on seasonal to interannual scales

The analysis shows that ridge keel depth distributions exhibit pronounced spatial and temporal variability. Examples of these empiric distributions for F11 and F14 shown as 1-CDF plots of the probability of exceeding a given keel depth in different deployment periods are found in Fig. S3. The figure indicates that a shifted exponential PDF provides a reasonable fit across most of the observed keel depth range, with some deviations for the shallowest (within 2-3 m) and the deepest (deeper than 15-20 m) ridge keels.

The series-average median keel depths vary within 4.1-4.7 m (Table 2), with median keel depth increasing westward. A similar tendency is observed for the deeper keels in the tail of the keel depth PDF, as expressed by the 99^{th} percentile of the empiric PDF which increases from 12.1 m at F11 to 13.4 m at F14. The deepest keels observed in the Fram Strait can protrude down to a 25-30 m depth, but these events are rare (a few objects per deployment season), though with a higher likelihood to be observed at F14 (6.5° W) than at F11 (3° W). One can speculate that objects with keels that deep could be either large pressure ridges or small icebergs from the Greenland ice sheet. However, we did not attempt to discriminate between the two in this study, given the number of these are relatively low.

The seasonal cycle of median keel drafts calculated from monthly data subsets pooled from all deployment seasons shows a weak tendency toward deeper keels in late winter-early spring and shallower keels in late summer-early fall (see Fig. 8). The magnitude of the seasonal cycle also increases westward, along with aforementioned tendency for the keels to be deeper on average at F14 than at F11. This tendency is even more pronounced for the tail of the keel depth distribution depicted here via the 99th percentile of the monthly empiric PDF of ridge keel depths. Although the choice of the 99th percentile threshold



290

295

300

305

310

315



can be considered somewhat arbitrary, it highlights well the seasonal variability and, at the same time, filters out objects more likely to be e.g. icebergs.

Figure 8 further shows the seasonal curve of the rate parameter λ of the fitted shifted exponential PDF derived using the MLE for monthly subsets of ridge keel drafts. In order to minimize the influence on the fit of infrequent objects beyond the break point in the tail of the distribution, typically with a keel depth deeper than 15 m (see Fig. S3), the fit was limited to the ridges shallower than this threshold. The variability in λ mirrors the pattern of variability in the 99^{th} percentile of ridge drafts, as for the exponential PDF decrease in the rate parameter is associated with a heavier tale of the probability density, hence in this case with a higher likelihood/frequency of deeper ridges.

The inferred seasonal variability is in line with a known seasonality of dynamic-thermodynamic drivers of a seasonal cycle of Arctic sea ice. More intense atmosphere-driven winter sea ice dynamics together with presence of younger ice types promotes ice ridge formation and deepening, while during summer melt ice ridges were found to melt faster than level ice (Perovich et al., 2003; Amundrud et al., 2006; Shestov et al., 2018; Salganik et al., 2023). Compared with F11 located at the eastern flank of the mooring array, the F14 mooring tracks the ice that with a higher likelihood originates from the central Arctic and Canadian Arctic and hence might have experienced a longer deformation history (Sumata et al., 2023; Krumpen et al., 2025) with less summer melt, leading to the registered keels to be generally deeper. One should also note that a seasonal cycle at F11 can be masked by a significant interannual variability due to proximity of the site to the frontal zones of the Fram Strait, with surface westward intrusions of warm and saline Atlantic Water or mixed waters promoting intense sea ice melt episodes even in winter. The frequency of these events was found to increase over the recent two decades (de Steur et al., 2023) with implications for sea ice cover.

On the scale of the entire series we find a substantial interannual variability in ridge keel depth PDF and hence maximum possible observed keel drafts (Figure 9). Along with monthly level ice thickness variations, there is a clear coherence in the series of monthly median keel drafts as well as 99th percentile of ridge drafts observed between the moorings. In particular one can discern a remarkable decrease in these values observed in all four moorings between summer 2017-early spring of 2019. This period overlaps with a strong decline in sea ice outflow through Fram Strait observed in 2018 and found to be unprecedented since 1990s. This decline has been linked to persistent regional atmospheric circulation anomalies, which prolonged ice residence time and intensified sea ice melt north of the strait (Sumata et al., 2022).

The variability of monthly rate parameter λ of shifted exponential PDF summarizes observed changes in ridge keel depth distribution. All four series demonstrate λ increasing with time, which is more pronounced in F11 and F12 and less for F14. These changes also reflect a tendency to an increased fraction of shallow ridges (Figure 7), which tends to be generally higher at F11 compared to the moorings located more to the west.

3.5 Interannual variation in the areal and volume contributions of sea-ice ridges

320 The general statistics on sea-ice ridges in Fram Strait inferred from the acquired data is further summarized in Table 2. The fractional areal contribution of ridges is calculated as the ratio of a cumulative ridge width to a total length (distance) of sea ice



325

330

335

340

345

350

355



that drifted over the mooring over the time interval of interest. In a similar fashion, the sum of all ice draft profiles identified as ridges is divided by a total profile of sea ice to derive a fractional contribution of ridges into the total sea-ice volume budget.

The true orientation of individual ridges relative to sea-ice drift and hence their true widths and keel depths profiles are unavailable. However, averaging over substantially long segments of sea-ice cover where an assumption of anisotropy in sea-ice surface morphology can be applied should keep the proportions between the areal and volume fractions of different ice categories inferred from linear profiles invariant to drift directions.

The monthly areal ridge fraction and fractional volume generally follows the variability in ridge counts (Figure 10) and shows an east to west gradient in both quantities. The series-average fractional ridge coverage increases from about 0.2 to 0.3 between F11 and F14 (see Table 2), with variability typically within 0.1 to 0.4 (\pm SD) of ice area. These values are similar to the ridge fraction estimates for Arctic sea ice made both in the past and more recently (e.g. Melling and Riedel, 1996; Hansen et al., 2014; Brenner et al., 2021; von Albedyll et al., 2022; Krumpen et al., 2025).

Figure 10 demonstrates that sea-ice ridges contribute significantly to the overall sea-ice volume and hence sea-ice volume transport through Fram Strait. The series-average estimates based on the mooring data suggest a volume fraction of 0.4 to 0.55 of ridged ice (ranging from 0.25 to 0.7 within $\pm SD$). In line with the longitudinal gradient in the number and coverage of ridges, on average there is a higher volume fraction of ridged ice at F14 compared to F11 (Table 2). We note that these results on the volume contribution should be considered as being close to the upper limit, as for simplification a ridge macroporosity of zero, i.e. an assumption of fully consolidated ridges or ridges with no air-, snow, or water-filled voids between the ice blocks, was assumed. While this assumption is generally valid for old ridges, FYI ridges especially in winter and spring are less consolidated. Recent analysis of available literature (Guzenko et al., 2023; Salganik et al., 2023; Maus, 2025), suggests an average bulk macroporosity of about 30% in winter and spring, with more consolidated ridges, and hence lower macroporosity, in summer. Given an ongoing decline in the fraction of older ice in the Arctic and transition to a more seasonal sea-ice cover, the fraction of FYI ridges is projected to increase. This increases the role of seasonal variability in macroporosity for making more accurate estimates of mass balance of Arctic sea ice. Figure 10 attempts to account for this, by showing the ridged ice volume fraction as an envelope, with higher and lower parts of the envelope calculated based on 0% and 30% macroporosity, respectively.

Analysis of ridge keel profiles distributions suggest that shallow ridges make a substantial contribution to the total volume balance of ridged ice. Figures S5 and S6 show CDF of volume contribution for ridges with different maximum keel drafts both as monthly variations during the study period as well as a series-long aggregates. Shallow ridges with keels smaller than 5 m deep contain typically about 40% of ridged sea-ice with this fraction increasing from F14 to F11 (Fig. S6). Most of the ridged ice, about 85% on average, is stored in sea ice ridges with keels below 10 m deep. Figure S5 demonstrates that in agreement with the increasing fraction of shallow ridges (see Fig. 7) their volume contribution tend to grow as well though shortness of the series as well as data gaps prevent us from making quantitative assessments of the respective trends.

Although ridge sails are not considered in these calculations, their volumetric and ridge mass balance contributions are much smaller than those of the keel. Under the assumption of hydrostatic equilibrium, sails typically account for not more than 10% of the total ice ridge volume or mass. On the other hand, a substantial fraction of ice was not categorized as ridges or level ice





(Figure 3), and some of this ice is deformed ice (e.g. rubble fields). Thus, some ridged or deformed ice is excluded, when only including distinct ridge keels.

Both fractional coverage and volume of ice ridges indicate a decline over the study period at all four sites. However, statis-360 tically significant linear changes are only found for the fraction of ridged ice volume at F11, which can be associated with the more consistent data coverage available for this mooring.

4 Conclusions

365

370

380

385

We analyzed seven years of sea-ice draft observations in the Arctic outflow in the Fram Strait, from September 2012 to September 2019, collected from upward-looking sonar (ULS) instruments with coincident ice drift velocity data from Acoustic Doppler Current Profilers (ADCPs). This allowed us to convert the time series of sea-ice draft into spatially uniform data series referenced relative to the moving sea-ice surface. The data set covers approximately 150 000 km of drifting Arctic sea ice across the Fram Strait, observed at four mooring sites located between 3°W and 6.5°W at 78.83°N. This provides the most extensive data set on spatially referenced sea-ice draft from the Atlantic sector of the Arctic Ocean, since the submarine surveys conducted earlier in the region (e.g. Williams et al., 1975; Wadhams, 1981, 1992).

With a spatial resolution of one meter, the sea-ice draft records were suitable for the application of sea-ice ridge and level ice detection algorithms. Unlike traditional methods that rely on a fixed 2.5 m level ice thickness threshold to isolate ridges (e.g. Wadhams and Horne, 1980; Ekeberg et al., 2015), our modified approach defines the level-ice draft locally from the data itself similar to the methodology recently used by Brenner et al. (2021) in the Beaufort Sea. This improves the flexibility of the ridge detection procedure, particularly in identifying shallow ridges, with keel drafts less than 5 m, that would likely be missed out by using a fixed threshold. Given the ongoing thinning of the Arctic sea-ice cover and the increasing seasonality of level ice thickness, both evident in our dataset and supported by recent studies (e.g. Sumata et al., 2023), adopting a dynamic threshold is justified.

Our analysis of ice draft data classified into level ice, ice ridges, and a residual mixed category, shows that level ice constitutes approximately 40-50% of the ice cover by area. The modal ice thickness ranged on average between 1 m and 2.5 m; ice thicknesses of 2.5 m or greater were seldom found. Thicker level ice was generally observed farther west, towards the East Greenland shelf. The study further reveals that sea-ice ridges constitute a significant portion of the sea-ice cover in the study area. Ridges occur frequently, with densities ranging, on average, from 6 to 9 individual ridges per kilometer of sea ice. This corresponds to approximately 3000 to 5500 ridges per month registered at each site. However, both ridge density and thus number of ridges exhibit large variability in time and between the sites. The fractional areal coverage of the sea-ice bottom surface by ridge keels averages between 0.2 and 0.3. In terms of volume, ridge keels represent an even greater proportion of the total sea-ice volume, with their fractional volume ranging from 0.28 to 0.55 across the four mooring sites. We find a westward increase in both ridge frequency and their corresponding areal coverage across the East Greenland Current. Although ridge sails are excluded from the present calculations, and the variable macroporosity of ridges remains a significant source of uncertainty, the results still underscore the important contribution of sea-ice ridges to the overall sea-ice volume budget. The



395

400



contribution from deformed ice might be even larger, given a fraction of the residual ice category, is likely to consist of e.g. rubble fields, and not detected as distinct ridge keels.

The relatively short duration of the time series limits our ability to conclude on temporal trends. Nonetheless, the data suggest a decline in the total number of ridges, accompanied by a general shallowing of ridge keels and consequently a reduction in their areal and volumetric contributions. This trend is most evident at the westernmost location, where the decline is more pronounced when the current results limited to ridges with keels drafts deeper than 5 m are considered along with previous analyses on ridge counts covering the period of 2007-2011 (Ekeberg et al., 2014).

The results also showcase the significant role of shallow ridges within the overall ridge distribution of the sea-ice cover of the Arctic outflow in Fram Strait. While large ridges are typically given more attention due to their impact as natural hazards for navigation and offshore infrastructure, smaller ridges emerge as important reservoirs of sea ice. These objects, which have often been excluded in earlier studies by using fixed thresholds, account for approximately 50–80% of all identified ridges and contribute an estimated 35–45% to the volume fraction of ridged ice, indicating their substantial contribution to the total budget of deformed ice. With continuous thinning of the Arctic sea-ice cover and the expected increase in the fraction of shallow ridges, they deserve greater attention in future studies.

Data availability. The data for the study will be made publicly available by the time of its publication.

405 Author contributions. DVD conceived the study and led the analysis. DVD developed and implemented the ridge detection algorithm. MAG and SG contributed to the interpretation of the results and validation of the methods. DVD and MAG contributed to the visualizations. All authors contributed to manuscript preparation, discussion of results, and critical revisions.

Competing interests. SG is a member of the editorial board of TC.

Acknowledgements. This study has been made possible by the long-term observations from the Fram Strait Arctic Outflow Observatory

410 maintained by the Norwegian Polar Institute (NPI). The sea-ice concentration data is from the EUMETSAT Ocean and Sea Ice Satellite
Application Facility (OSI SAF). The monthly mean sea-ice motion vectors are from the NASA National Snow and Ice Data Center Distributed
Active Archive Center (NSIDC) provided by the Integrated Climate Data Center (ICDC), University of Hamburg, Germany. The authors are
grateful to engineers and logistical personnel at the NPI for the dedicated work on servicing the moorings of the Fram Strait Arctic Outflow
Observatory. We would also like to thank the captains and crews of FF Lance and FF Kronprins Haakon for support and assistance with

415 recovery and deployment of the moorings, often during challenging conditions.





References

- Amundrud, T. L., Melling, H., Ingram, R. G., and Allen, S. E.: The effect of structural porosity on the ablation of sea ice ridges, J. Geophys. Res., 111, C06 004, https://doi.org/10.1029/2005JC002895, 2006.
- Arnold, B. C.: Pareto Distributions, International Cooperative Publishing House, Fairland, MD, 1990.
- 420 Arya, S. P. S.: Contribution of form drag on pressure ridges to the air stress on Arctic ice, J. Geophys. Res., 78, 7092–7099, https://doi.org/10.1029/JC078I030P07092, 1973.
 - Brenner, S., Rainville, L., Thomson, J., Cole, S., and Lee, C.: Comparing Observations and Parameterizations of Ice Ocean Drag Through an Annual Cycle Across the Beaufort Sea, J. Geophys. Res.-Oceans, 126, e2020JC016977, https://doi.org/10.1029/2020JC016977, 2021.
- Castellani, G., Lüpkes, C., Hendricks, S., and Gerdes, R.: Variability of Arctic sea-ice topography and its impact on the atmospheric surface drag, J. Geophys. Res. Oceans, 119, 6743–6762, https://doi.org/10.1002/2013JC009712, 2014.
 - de Steur, L., Sumata, H., Divine, D. V., Granskog, M. A., and Pavlova, O.: Upper ocean warming and sea ice reduction in the East Greenland Current from 2003 to 2019, Commun. Earth Env., 4, 261, https://doi.org/10.1038/s43247-023-00913-3, 2023.
 - Duncan, K. and Farrell, S. L.: Determining Variability in Arctic Sea Ice Pressure Ridge Topography With ICESat-2, Geophys. Res. Lett., 49, e2022GL100 272, https://doi.org/10.1029/2022GL100272, 2022.
- Ekeberg, O.-C., Høyland, K., Hansen, E., and Tschudi, M.: Reduction in the Number and Draft of Ridges in the Transpolar Drift in the Fram Strait during 2006-2011, in: Proceedings of the 22nd International Conference on Port and Ocean Engineering under Arctic Conditions, p. 1226, https://doi.org/10.3850/978-981-09-0750-1_1226, 2014.
 - Ekeberg, O.-C., Høyland, K., and Hansen, E.: Ice ridge keel geometry and shape derived from one year of upward looking sonar data in the Fram Strait, Cold Reg. Res. Tech., 109, 78–86, https://doi.org/10.1016/j.coldregions.2014.10.003, 2015.
- 435 Fernández-Méndez, M., Olsen, L. M., Kauko, H. M., Meyer, A., Rösel, A., Merkouriadi, I., Mundy, C. J., Ehn, J. K., Johansson, A. M., Wagner, P. M., Ervik, Å., Sorrell, B. K., Duarte, P., Wold, A., Hop, H., and Assmy, P.: Algal Hot Spots in a Changing Arctic Ocean: Sea-Ice Ridges and the Snow-Ice Interface, Front. Mar. Sci., 5, 75, https://doi.org/10.3389/fmars.2018.00075, 2018.
 - Fissel, D. B., Marko, J. R., and Melling, H.: Advances in upward looking sonar technology for studying the processes of change in Arctic Ocean ice climate, J. Oper. Oceanogr., 1, 9–18, https://doi.org/10.1080/1755876X.2008.11081884, 2008.
- Gradinger, R., Bluhm, B., and Iken, K.: Arctic sea-ice ridges—Safe heavens for sea-ice fauna during periods of extreme ice melt?, Deep Sea Res. II, 57, 86–95, https://doi.org/10.1016/j.dsr2.2009.08.008, 2010.
 - Guzenko, R. B., Mironov, Y. U., May, R. I., Porubaev, V. S., Kovalev, S. M., Khotchenkov, S. V., Kornishin, K. A., and Efimov, Y.: Morphometry and Internal Structure of Ice Ridges and Stamukhas in the Kara, Laptev and East Siberian Seas: Results of 2013–2017 Field Studies, SSRN Electronic Journal, https://doi.org/10.2139/ssrn.4359510, [preprint], 2023.
- Hansen, E., Gerland, S., Granskog, M. A., Pavlova, O., Renner, A. H. H., Haapala, J., Lœyning, T. B., and Tschudi, M.: Thinning of Arctic sea ice observed in Fram Strait: 1990-2011, J. Geophys. Res.-Oceans, 118, 5202–5221, https://doi.org/10.1002/jgrc.20393, 2013.
 - Hansen, E., Ekeberg, O.-C., Gerland, S., Pavlova, O., Spreen, G., and Tschudi, M.: Variability in categories of Arctic sea ice in Fram Strait, J. Geophys. Res.-Oceans, 119, 7175–7189, https://doi.org/10.1002/2014JC010048, 2014.
- Hansen, E., Ervik, Å., Eik, K., Olsson, A., and Teigen, S. H.: Long-term observations (2014-2020) of level ice draft, keel depth and ridge frequency in the Barents Sea, Cold Reg. Res. Tech., 216, 103 988, https://doi.org/10.1016/j.coldregions.2023.103988, 2023.
 - JCOMM Expert Team on Sea Ice: WMO sea-ice nomenclature, Nomenclature WMO-No. 259, World Meteorological Organization, Geneva, 2015.



470



- Kacimi, S. and Kwok, R.: Arctic snow depth, ice thickness, and volume from ICESat-2 and CryoSat-2: 2018–2021, Geophys. Res. Lett., 49, e2021GL097 448, https://doi.org/10.1029/2021GL097448, 2022.
- Kortum, K., Singha, S., Spreen, G., Hutter, N., Jutila, A., and Haas, C.: SAR deep learning sea ice retrieval trained with airborne laser scanner measurements from the MOSAiC expedition, Cryosph., 18, 2207–2222, https://doi.org/10.5194/tc-18-2207-2024, 2024.
 - Krumpen, T., von Albedyll, L., Bünger, H. J., Castellani, G., Hartmann, J., Helm, V., Hendricks, S., Hutter, N., Landy, J. C., Lisovski, S., Lüpkes, C., Rohde, J., Suhrhoff, M., and Haas, C.: Smoother sea ice with fewer pressure ridges in a more dynamic Arctic, Nat. Clim. Change, 15, 66–72, https://doi.org/10.1038/s41558-024-02199-5, 2025.
- 460 Lu, P., Li, Z., Cheng, B., and Leppäranta, M.: A parameterization of the ice-ocean drag coefficient, J. Geophys. Res., 116, 1–14, https://doi.org/10.1029/2010JC006878, 2011.
 - Maus, S.: Bounds on the initial macroporosity of sea ice pressure ridges, Ann. Glaciol., 66, e10, https://doi.org/10.1017/aog.2025.4, 2025.
 - Maykut, G. and Untersteiner, N.: Some Results from a Time-Dependent Thermodynamic Model of Sea Ice, J. Geophys. Res., 76(6), 1550–1575, 1971.
- Mchedlishvili, A., Lüpkes, C., Petty, A., Tsamados, M., and Spreen, G.: New estimates of pan-Arctic sea ice–atmosphere neutral drag coefficients from ICESat-2 elevation data, Cryosph., 17, 4103–4131, https://doi.org/10.5194/tc-17-4103-2023, 2023.
 - McLaren, A. S.: Analysis of the under-ice topography in the Arctic Basin as recorded by the USS Nautilus during August 1958, Arct., 41, 117–126, https://doi.org/10.14430/arctic1703, 1988.
 - McLaren, A. S.: The under-ice thickness distribution of the Arctic Basin as recorded in 1958 and 1970, J. Geophys. Res.-Oceans, 94, 4971–4983, https://doi.org/10.1029/JC094iC04p04971, 1989.
 - Melling, H. and Riedel, D. A.: The underside topography of sea ice over the continental shelf of the Beaufort Sea in the winter of 1990, J. Geophys. Res.-Oceans, 100, 13 641–13 653, https://doi.org/10.1029/95JC00309, 1995.
 - Melling, H. and Riedel, D. A.: Development of seasonal pack ice in the Beaufort Sea during the winter of 1991-1992: A view from below, J. Geophys. Res.-Oceans, 101, 11,975–11,991, https://doi.org/10.1029/96JC00284, 1996.
- Melling, H., Johnston, P. H., and Riedel, D. A.: Measurements of the Underside Topography of Sea Ice by Moored Subsea Sonar, J. Atmos. Oce. Tech., 12, 589–602, https://doi.org/10.1175/1520-0426(1995)012<0589:MOTUTO>2.0.CO;2, 1995.
 - OSI SAF: Global sea ice concentration climate data record 1978-2020 (v3.0, 2022), EUMETSAT Ocean and Sea Ice Satellite Application Facility (OSI SAF), https://doi.org/10.15770/EUM_SAF_OSI_0013, (Data extracted from EUMETSAT Data Centre: (1990-2020, Northern Hemisphere), accessed on 15-Jan-2025), 2022.
- 480 Perovich, D. K., Grenfell, T. C., Richter-Menge, J. A., Light, B., Tucker III, W. B., and Eicken, H.: Thin and thinner: sea ice mass balance measurements during SHEBA, J. Geophys. Res.-Oceans, 108, https://doi.org/10.1029/2001JC001079, 2003.
 - Polojärvi, A., Tuhkuri, J., and Hendrikse, H.: Sea ice from an engineer's perspective, in: Sea Ice: Its Physics, Chemistry, Biology, Geology and Societal Importance, edited by Thomas, D. N., chap. 4, pp. 147–176, Wiley, Hoboken, NJ, 4th edn., 2025.
- Richter-Menge, J., Druckenmiller, M. L., Jeffries, M. O., et al.: Arctic Report Card 2019: Sea Ice, Bulletin of the American Meteorological

 Society, 100, –, https://doi.org/10.25923/bw4d-my28, includes the "Sea Ice" section in the 2019 Arctic Report Card (NOAA / Office of Oceanic and Atmospheric Research), 2019.
 - Ricker, R., Fons, S., Jutila, A., Hutter, N., Duncan, K., Farrell, S. L., Kurtz, N. T., and Fredensborg Hansen, R. M.: Linking scales of sea ice surface topography: evaluation of ICESat-2 measurements with coincident helicopter laser scanning during MOSAiC, Cryosph., 17, 1411–1429, https://doi.org/10.5194/tc-17-1411-2023, 2023.



495



- 490 Salganik, E., Lange, B. A., Katlein, C., Matero, I., Anhaus, P., Muilwijk, M., Høyland, K. V., and Granskog, M. A.: Observations of preferential summer melt of Arctic sea-ice ridge keels from repeated multibeam sonar surveys, Cryosph., 17, 4873–4887, https://doi.org/10.5194/tc-17-4873-2023, 2023.
 - Samardžija, I. and Høyland, K. V.: Analysis of the relationship between level ice draft, ridge frequency and ridge keel draft for use in the probabilistic assessment of ice ridge loads on offshore structures, Oce. Engin., 270, 113 593, https://doi.org/10.1016/j.oceaneng.2022.113593, 2023.
 - Shestov, A., Høyland, K., and Ervik, Å.: Decay phase thermodynamics of ice ridges in the Arctic Ocean, Cold Reg. Sci. Tech., 152, 23–34, https://doi.org/10.1016/j.coldregions.2018.04.005, 2018.
 - Spreen, G., de Steur, L., Divine, D., Gerland, S., Hansen, E., and Kwok, R.: Arctic Sea Ice Volume Export Through Fram Strait From 1992 to 2014, J. Geophys. Res. Oceans, 125, e2019JC016039, https://doi.org/l0.1029/2019JC016039, 2020.
- 500 Sterlin, J., Tsamados, M., Fichefet, T., Massonnet, F., and Barbic, G.: Effects of sea ice form drag on the polar oceans in the NEMO-LIM3 global ocean–sea ice model, Ocean Modelling, 184, 102 227, https://doi.org/10.1016/j.ocemod.2023.102227, 2023.
 - Sumata, H., de Steur, L., Gerland, S., Divine, D. V., and Pavlova, O.: Unprecedented decline of Arctic sea ice outflow in 2018, Nat. Commun., 13, 1747, https://doi.org/10.1038/s41467-022-29470-7, 2022.
- Sumata, H., de Steur, L., Divine, D. V., Granskog, M. A., and Gerland, S.: Regime shift in Arctic Ocean sea ice thickness, Nature, 615, 443–449, https://doi.org/10.1038/s41586-022-05686-x, 2023.
 - Tan, B., Li, Z.-J., Lu, P., Haas, C., and Nicolaus, M.: Morphology of sea ice pressure ridges in the northwestern Weddell Sea in winter, J. Geophys. Res.-Oceans, 117, C06024, https://doi.org/10.1029/2011JC007800, 2012.
 - Timco, G. and Burden, R.: An analysis of the shapes of sea ice ridges, Cold Reg. Res. Tech., 25, 65–77, https://doi.org/10.1016/S0165-232X(96)00017-1, 1997.
- 510 Tsamados, M., Feltham, D. L., Schroeder, D., Flocco, D., Farrell, S. L., Kurtz, N., Laxon, S. W., and Bacon, S.: Impact of Variable Atmospheric and Oceanic Form Drag on Simulations of Arctic Sea Ice, J. Phys. Ocean., 44, 1329–1353, https://doi.org/10.1175/JPO-D-13-0215.1, 2014.
- Tschudi, M., Meier, W. N., Stewart, J. S., Fowler, C., and Maslanik, J.: Monthly mean sea-ice motion vectors derived from Polar Pathfinder Daily 25 km EASE-Grid Sea Ice Motion Vectors, Version 4.1. Boulder, Colorado USA. NASA National Snow and Ice Data Center Distributed Active Archive Center., https://doi.org/10.5067/INAWUWO7QH7B, [last access date: October 21, 2024] were provided in netCDF format (file version fv0.01) by the Integrated Climate Data Center (ICDC, https://www.cen.uni-hamburg.de/icdc) University of Hamburg, Hamburg, Germany., 2024.
 - Tukey, J. W.: Exploratory Data Analysis, Addison-Wesley, Reading, Massachusetts, 1977.
- Valenti, V., Mahoney, A., and Metzger, A.: A probabilistic description of pressure ridge width, spacing, and keel depth for the Chukchi and Beaufort seas based on IPS and ADCP observations, Cold Reg. Sci. Tech., 182, 103171, https://doi.org/10.1016/J.COLDREGIONS.2020.103171, 2021.
 - Vinje, T., Nordlund, N., and Kvambekk, Å.: Monitoring ice thickness in Fram Strait, J. Geophys. Res.-Oceans, 103, 10437–10449, https://doi.org/10.1029/97JC03360, 1998.
- von Albedyll, L., Hendricks, S., Grodofzig, R., Krumpen, T., Arndt, S., Belter, H. J., Birnbaum, G., Cheng, B., Hoppmann, M., Hutchings, J.,

 Itkin, P., Lei, R., Nicolaus, M., Ricker, R., Rohde, J., Suhrhoff, M., Timofeeva, A., Watkins, D., Webster, M., and Haas, C.: Thermodynamic and dynamic contributions to seasonal Arctic sea ice thickness distributions from airborne observations, Elementa Sci. Anthrop., 10, 00074, https://doi.org/10.1525/elementa.2021.00074, 2022.





- Wadhams, P.: Sea-ice topography of the Arctic Ocean in the region 70° W to 25° E, Phil. Trans. Roy. Soc. London. A., 302, 45–85, https://doi.org/10.1098/rsta.1981.0157, 1981.
- Wadhams, P.: The prediction of extreme keel depths from sea ice profiles, Cold Reg. Sci. Tech., 6, 257–266, https://doi.org/10.1016/0165-232X(83)90046-0, 1983.
 - Wadhams, P.: Evidence for thinning of the Arctic ice cover north of Greenland, Nature, 345, 795–797, https://doi.org/10.1038/345795a0, 1990.
- Wadhams, P.: Sea ice thickness distribution in the Greenland Sea and Eurasian Basin, May 1987, J. Geophys. Res.-Oceans, 97, 5331–5348, https://doi.org/10.1029/91JC03137, 1992.
 - Wadhams, P.: New predictions of extreme keel depths and scour frequencies for the Beaufort Sea using ice thickness statistics, Cold Reg. Sci. Tech., 76-77, 77–82, https://doi.org/10.1016/j.coldregions.2011.12.002, 2012.
 - Wadhams, P. and Davis, N. R.: Further evidence of ice thinning in the Arctic Ocean, Geophys. Res. Lett., 27, 3973–3975, https://doi.org/10.1029/2000GL011802, 2000.
- Wadhams, P. and Davy, T.: On the spacing and draft distributions for pressure ridge keels, J. Geophys. Res., 91, 10,697–10,708, https://doi.org/10.1029/JC091iC09p10697, 1986.
 - Wadhams, P. and Horne, R. J.: An Analysis Of Ice Profiles Obtained By Submarine Sonar In The Beaufort Sea, J. Glaciol., 25, 401–424, https://doi.org/10.3189/S0022143000015264, 1980.
- Wadhams, P., Hughes, N., and Rodrigues, J.: Arctic sea ice thickness characteristics in winter 2004 and 2007 from submarine sonar transects,

 J. Geophys. Res.-Oceans, 116, C00E02, https://doi.org/10.1029/2011JC006982, 2011.
 - Williams, E., Swithinbank, C., and de Q. Robin, G.: A Submarine Sonar Study of Arctic Pack Ice, J. Glaciol., 15, 349–362, https://doi.org/10.3189/S002214300003447X, 1975.



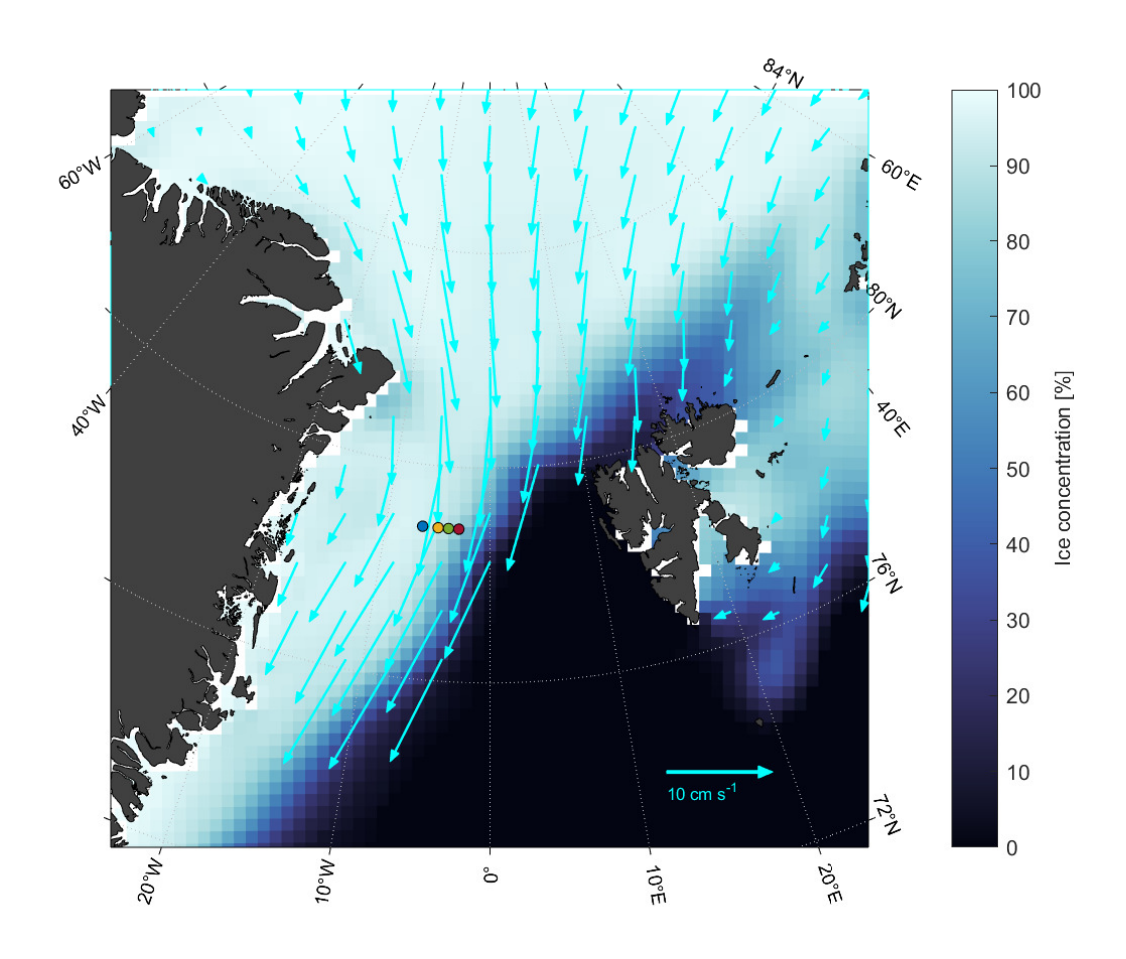


Figure 1. Location of the four moorings of the Fram Strait Arctic Outflow Observatory shown by filled circles. Color codes as in Fig. 2: red, green, yellow and blue for F11, F12, F13 and F14, respectively. Mean March sea-ice concentration (OSI SAF (2022), colorbar) and mean January to April sea-ice drift (Tschudi et al. (2024), arrows) in 2012-2019.





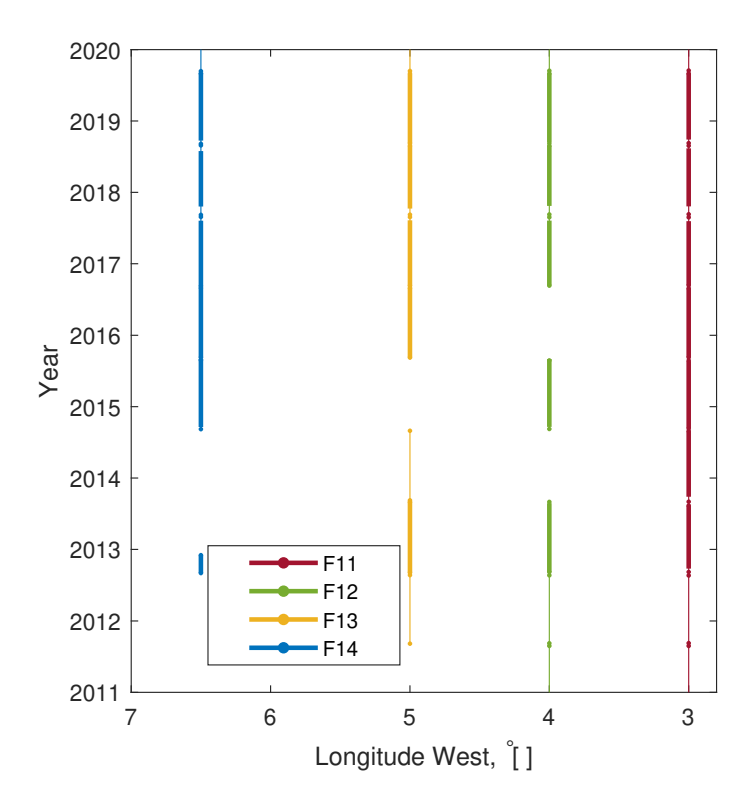


Figure 2. Overview of the temporal coverage of ULS data from the Fram Strait Arctic Outflow Observatory at 78.83°N between 3° and 7°W during 2019-2019. Thicker lines highlight the periods when the time series of ice drafts from IPS5 instruments and sea-ice velocity data from ADCPs were combined to produce spatial series of sea-ice draft. These series were analyzed for ridge and level ice statistics in the present study. Periods with ULS but no ADCP data are shown by thin lines. Note that the figure does not reflect minor changes in both latitudinal and longitudinal positions of the moorings that occurred between deployments.





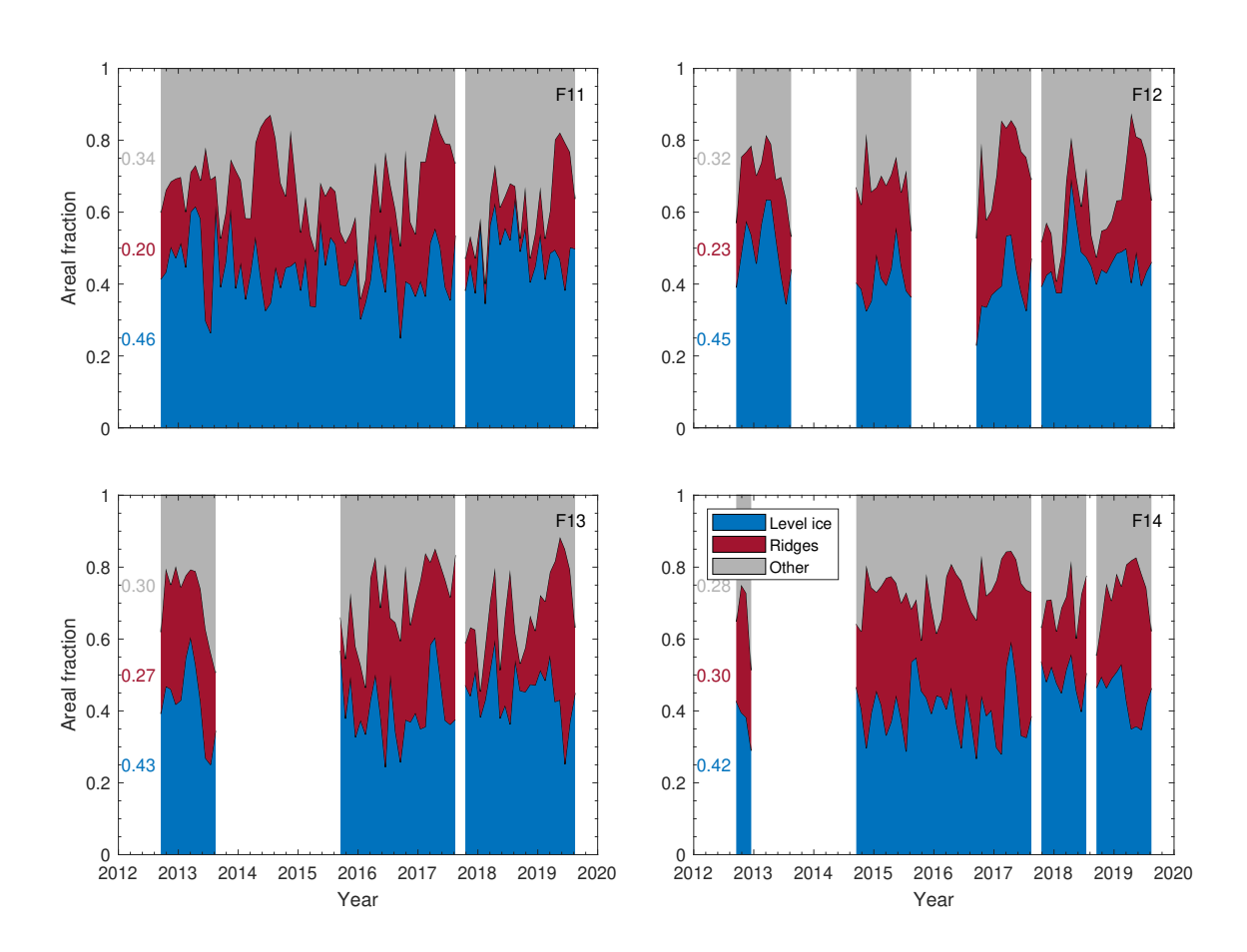


Figure 3. Monthly areal fractions of ice ridges, level ice and mixed ice category for the four moorings calculated relative to the total ice area. Multiannual means for each category and mooring are shown as numbers with colors matching the colors used for each specific category.





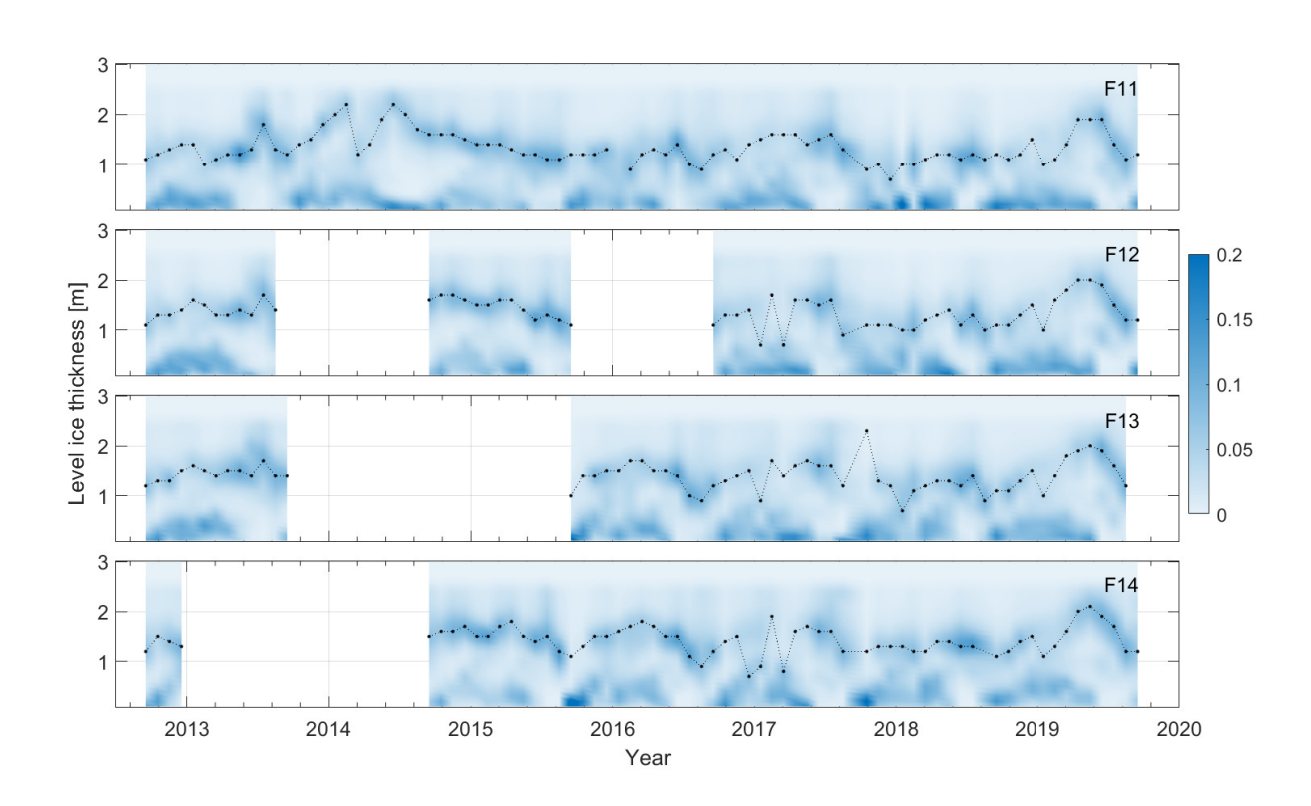


Figure 4. Monthly PDF of level ice thickness at the mooring sites (blue shading, see colorbar). Black dots and lines highlight the maxima in modal level ice thicknesses distribution associated with thicker FYI/MYI advected from the Arctic.





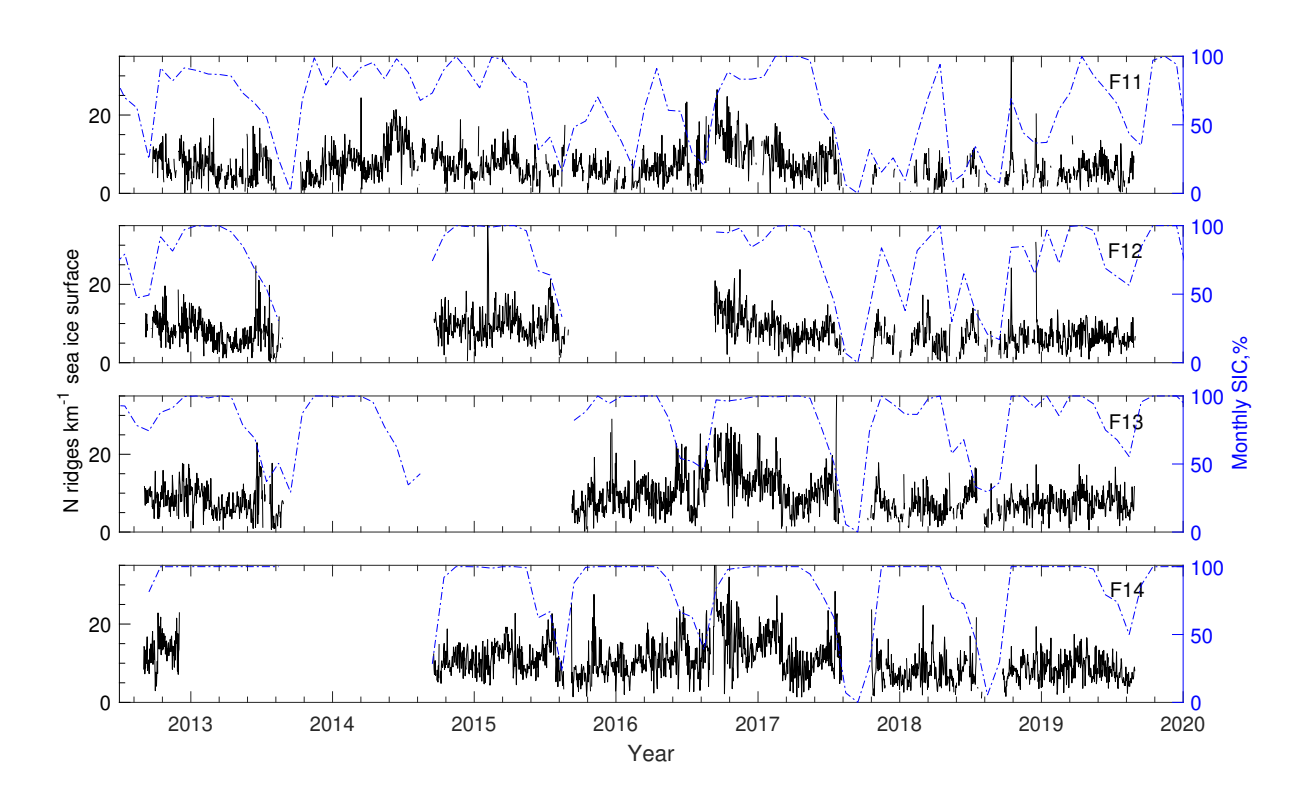


Figure 5. Daily effective ridge density defined as a number of ridges per kilometer of ice at the four mooring locations (black solid lines). Dash-dotted blue lines show monthly sea-ice concentration at the mooring sites calculated directly from the spatial ice draft data series as fraction of points identified as ice.





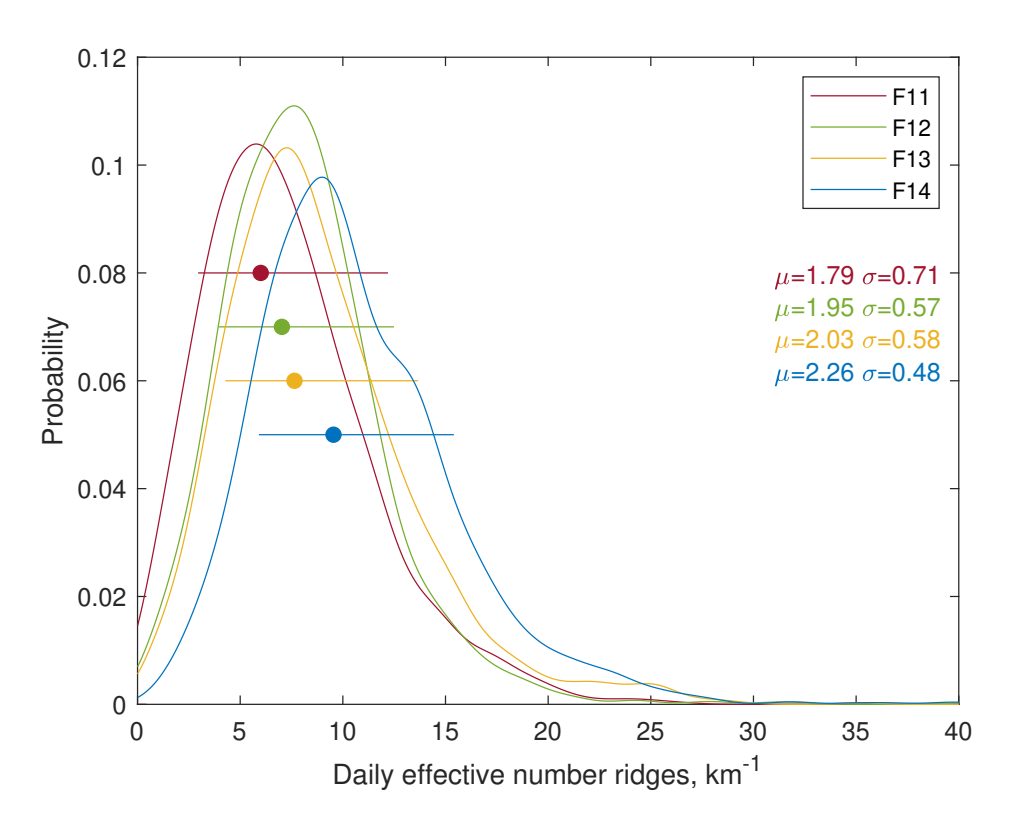


Figure 6. Empirical probability density function of daily effective ridge density (number of ridges per km of ice) at the four mooring locations during 2012-2019. Filled circles and horizontal lines show median ridge densities (e^{μ}) and the 68% prediction intervals of [$e^{\mu/\sigma}$, $e^{\mu*\sigma}$], respectively, calculated from the log-normal probability distribution fitted to the data. Parameters μ and σ of the fitted log-normal distributions are shown in the panel and highlighted with colors corresponding to colors of the respective labels.



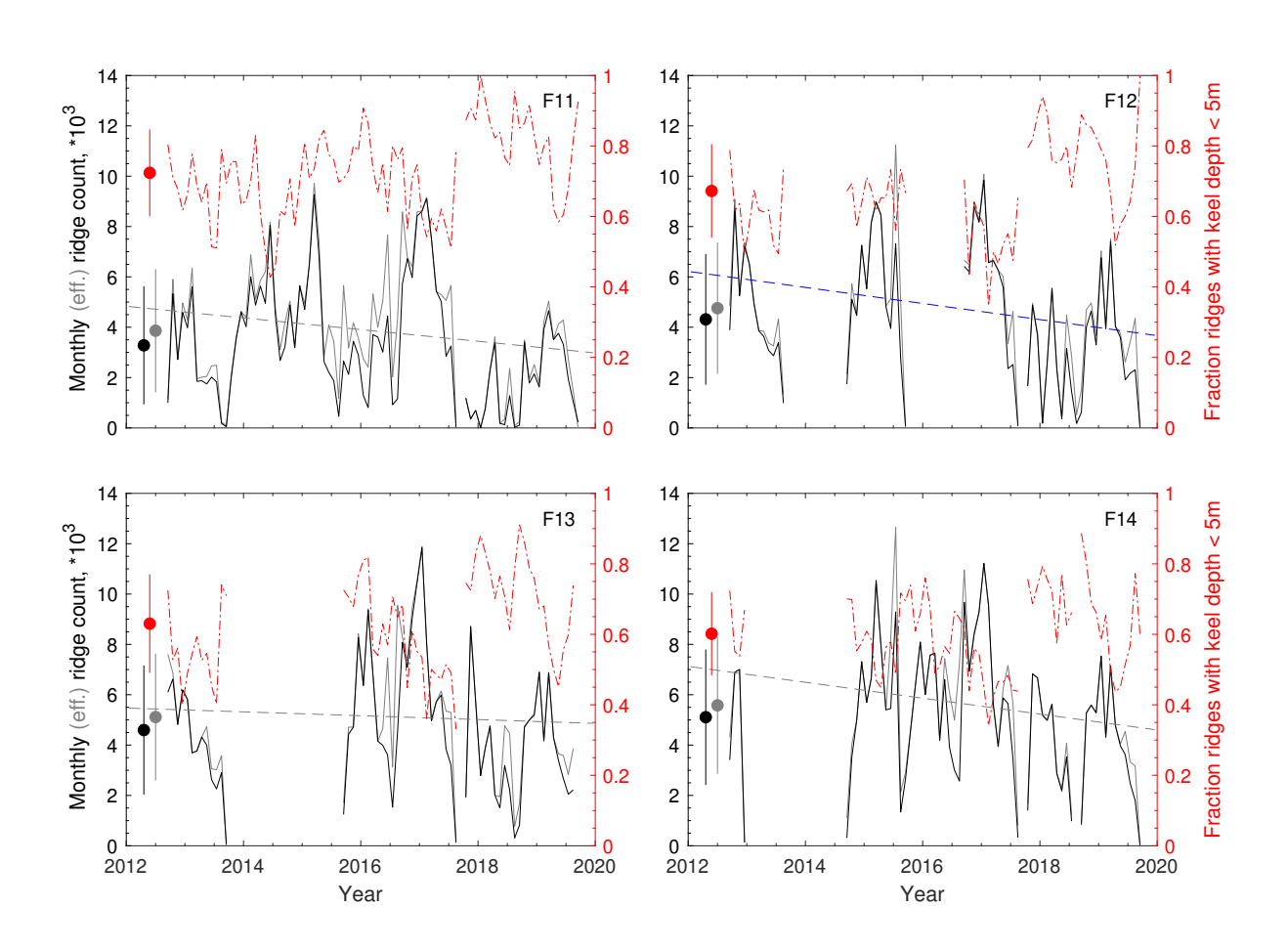


Figure 7. Monthly ridge count (black solid line), monthly effective ridge count (i.e. ridge count scaled by sea-ice concentration; gray solid line) and a fraction of shallow ridges with a keel depth less than 5 m at the four mooring locations. Filled circles with vertical lines show the respective multiannual means and standard deviations for these variables over the period of 2012-2019. Dashed lines show linear fits to the monthly effective ridge counts; statistically significant linear trend (p-value<0.05, F12 data alone) is highlighted blue.





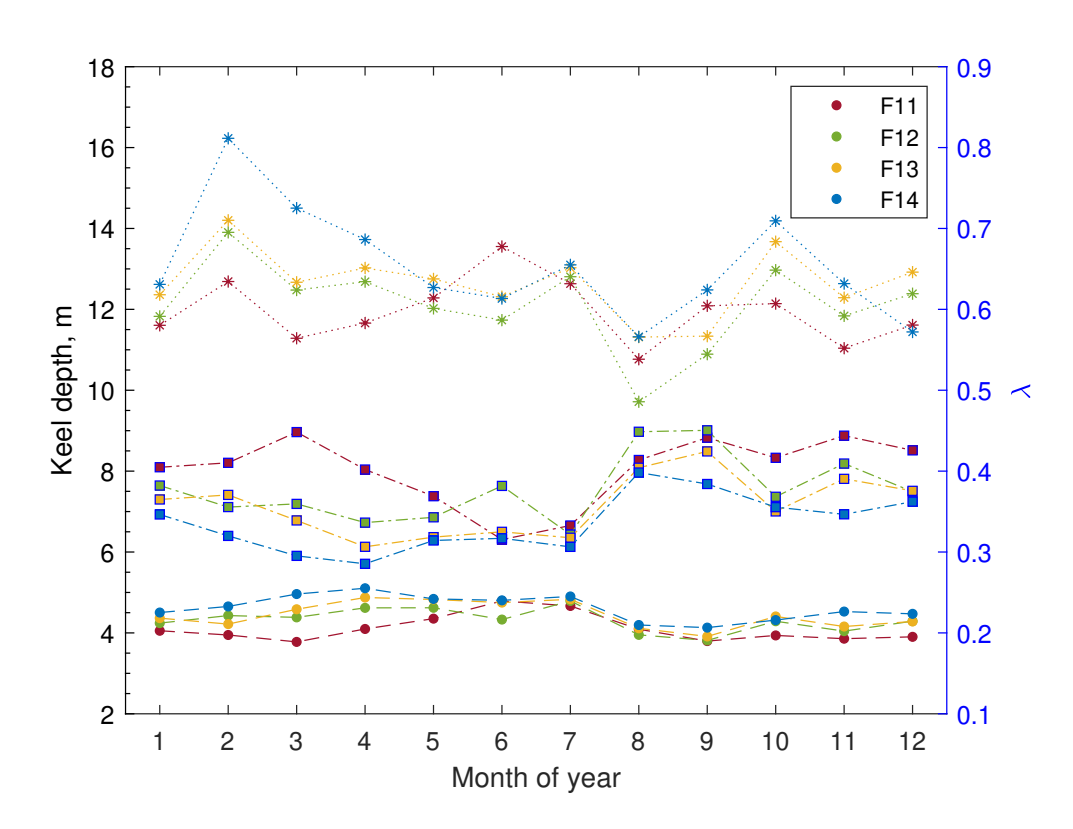


Figure 8. Seasonal variability of monthly sample median (shown by filled circles) and the sample 99^{th} percentile (asterisks) of keel depth at the four mooring locations during 2012-2019. Filled squares associated with the right y-axis show seasonal variability of rate parameter λ of the shifted exponential distribution fitted to monthly subsets of the ridge draft data.





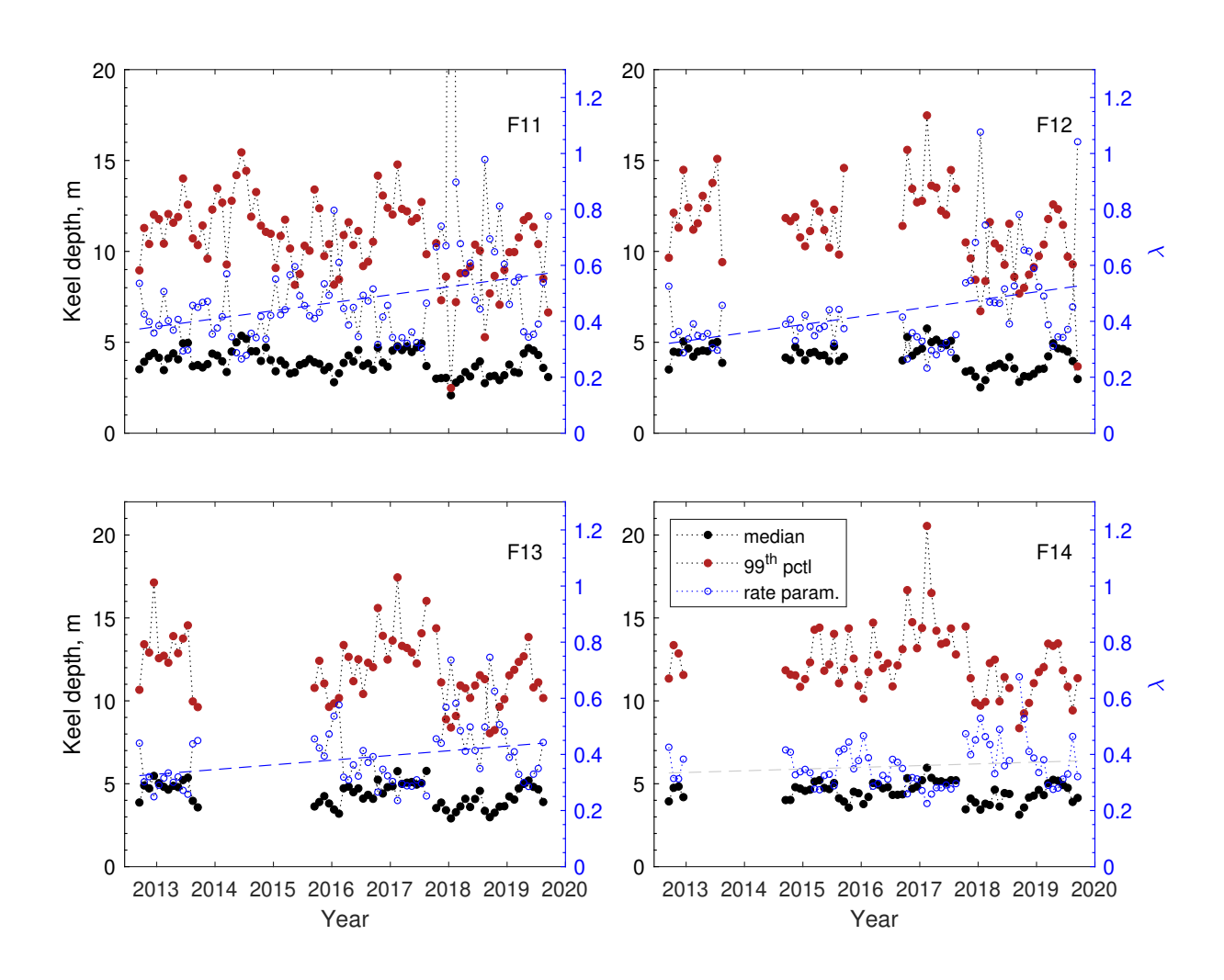


Figure 9. Left axis: monthly median and 99^{th} percentile of keel drafts at the four mooring locations during 2012-2019 shown with black and red filled circles and lines, respectively. Right axis: blue open circles and lines show monthly variability of rate parameter λ of the shifted exponential distribution fitted to the monthly subsets of the ridge keel draft data. Dashed lines show linear trends fitted to monthly λ ; statistically significant trends (p-value<0.05) are highlighted blue.





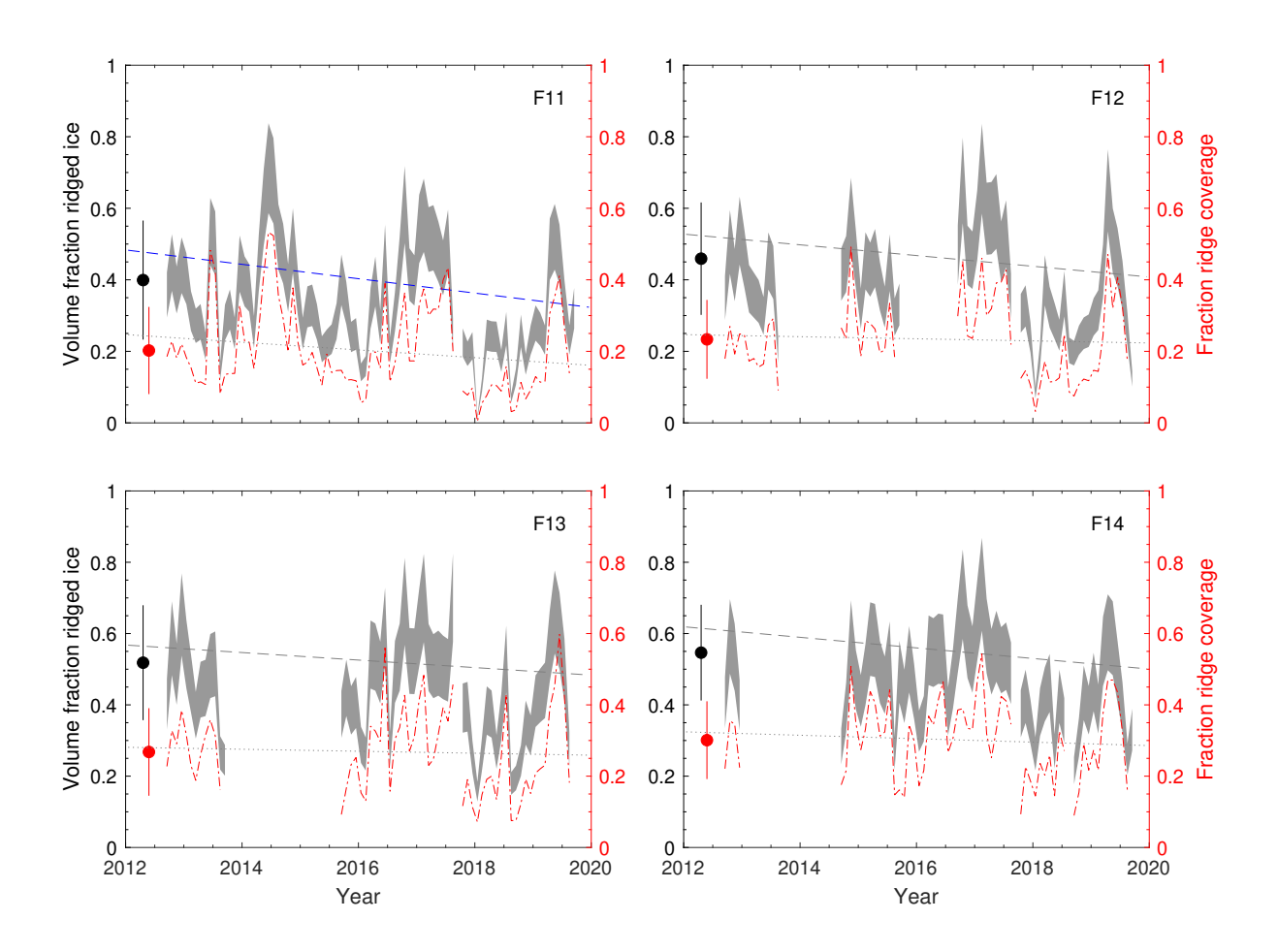
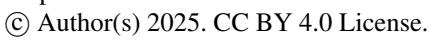


Figure 10. Monthly average of fractional ridge coverage (dash-dotted red line) and fractional ridged ice volume shown as grey envelope at the four mooring locations. Upper and lower parts of the envelope correspond to assumptions of fully consolidated ice ridges (i.e. 0% keel macroporosity) and 30% keel macroporosity, respectively, used in fractional ridged ice volume calculations. Filled circles with vertical lines show the respective multiannual means and standard deviations for these variables over the period of 2012-2019. Dotted and dashed lines show linear trends fitted to monthly fractional ridge coverage and fractional ridged ice volume, respectively; statistically significant trend (p-value<0.05, F11 ridged ice volume fraction only) is highlighted blue. Note that for calculating the multiannual mean volume fraction and trends an assumption of fully consolidated ice ridges (zero macroporosity) was used.







| Site | Longitude | Water depth, | Data record, | Data record, | Data record, |
|------|---------------|--------------|--------------|--------------|---------------|
| | $[^{\circ}W]$ | [m] | [km of ice] | [days] | [days of ice] |
| F11 | 3 | 2470 | 46564 | 2317 | 1552 |
| F12 | 4 | 1860 | 36582 | 1693 | 1355 |
| F13 | 5 | 1020 | 35843 | 1729 | 1445 |
| F14 | 6.5 | 270 | 33286 | 1763 | 1570 |

Table 1. Locations, depths, and the lengths of sea-ice records presented as a total distance of sea ice that drifted over the sites, the number of days with observations and the effective number of days of ice for the four taut-line moorings in Fram Strait along the 78.83°N latitude during 2012-2019. The effective number of days of ice is a number (sum) of days with ice observations weighted by daily ice concentrations calculated from the data. The mooring locations are typically accurate to within a fraction of a minute degree and varied slightly from year to year after the re-deployment, mainly driven by local sea-ice conditions and sea-ice drift at the time of deployment. The water depths at deployment locations could vary within a 10-20 m range accordingly. Note also the depth gradient between the mooring locations from about 2500 m (F11) in the east to less than 300 m (F14) on the continental shelf in the west.





| Site | Ridge | Fraction ridge | Fraction ridge | Ridge density, | Median (99 th prctl), |
|------|-------------------------------|-------------------------|------------------------|--------------------|----------------------------------|
| | $\operatorname{count}, *10^3$ | coverage $(\pm \sigma)$ | volume $(\pm \sigma)$ | km^{-1} | keel depth, m |
| F11 | 276 | 0.20 (0.12) | 0.28(0.12)-0.40 (0.17) | 6.0 (3.0,12.2) | 4.1 (12.1) |
| F12 | 263 | 0.23 (0.11) | 0.32(0.11)-0.46 (0.16) | 7.0 (4.0,12.5) | 4.4 (12.4) |
| F13 | 276 | 0.27 (0.12) | 0.36(0.11)-0.46 (0.16) | 7.7 (4.3,13.7) | 4.4 (12.8) |
| F14 | 322 | 0.30 (0.11) | 0.38(0.09)-0.55 (0.13) | 9.6 (5.9,15.4) | 4.7 (13.4) |

Table 2. Summary statistics on sea-ice ridges in Fram Strait from sea-ice data acquired by the four moorings during 2012-2019. Total ridge count is rounded to the nearest thousand. Median ridge density (median number of ridges per kilometer of sea-ice cover) and its 68% prediction intervals were calculated for log-normal probability distribution fitted to the data. The average fractional ridge volume is provided as a range calculated from the assumptions of 30% (lower estimate) to 0% (upper estimate) ridge keel macroporosity, respectively.